

Experimental insights on crystal chemistry of high-Ti garnets from garnet-melt partitioning of rare-earth and high-field-strength elements

RACHEL E. DWARZSKI,* DAVID S. DRAPER, CHARLES K. SHEARER, AND CARL B. AGEE

Institute of Meteoritics, Department of Earth and Planetary Sciences, University of New Mexico, Albuquerque, New Mexico 87131, U.S.A.

ABSTRACT

High-temperature experiments were performed from 3.0 to 7.0 GPa to investigate the effect of composition on near-liquidus garnet-melt trace-element partition coefficients (D -values) in a Ti- and Fe-rich lunar bulk composition. Starting compositions were doped with Sc, Sr, Y, Zr, Ba, Nd, Sm, Dy, Yb, Hf, and Th. D -values were measured by ion-microprobe analysis. The lattice strain model of Blundy and Wood (1994) was applied to measured D -values, and then compared with the predictive garnet-melt trace-element partitioning model of van Westrenen et al. (2001b). Although the lattice-strain model describes our data adequately, there is a substantial mismatch between the prediction of the van Westrenen et al. (2001b) model and the actual measured D -values. We suggest crystal-chemical effects associated with the high Ti content of our experimental garnets may be responsible for this mismatch. Titanium alone does not appear to control partitioning; we infer that Fe^{2+} and/or Mg^{2+} are required to partition into octahedral coordination on the Y-site, which may further necessitate Si^{4+} to also partition on the Y-site for charge balance. This combination of effects influences trace-element partitioning in the garnet. Observed changes in D -values correlate with the integration of Ti on the Y-site in a majorite-like exchange, yet our garnets incorporate little or no majorite. Garnets grown have some of the lowest apparent Young's modulus values (274–528 GPa) yet documented for the garnet X-site indicating higher compressibilities than previously inferred.

Keywords: Experimental petrology, high-pressure experiments, trace elements and REE, garnet-melt partitioning, major and minor elements, titanium, crystal chemistry

INTRODUCTION

Garnet is a major rock-forming mineral whose geochemical signature has been used to investigate and constrain petrogenetic processes within planetary interiors. Garnet preferentially incorporates the heavy rare earth elements (HREE) compared with the light rare earth elements (LREE), imparting the characteristic “garnet signature” to liquids formed from garnet-bearing source regions. Although it has been well established that composition, pressure, temperature, crystal chemistry, and oxygen fugacity affect garnet-melt partitioning in Mg-rich terrestrial compositions, there are fewer experimental constraints on partitioning in Fe-rich compositions relevant to other terrestrial planets. In addition, the detailed effects of crystal chemistry on garnet-melt partitioning in Fe-rich systems have not yet been explored fully and are therefore only partially understood. Understanding the partitioning of trace elements between garnet and melt is essential, as accurate and appropriate D -values are crucial for modeling petrogenetic processes in planetary interiors.

Onuma et al. (1968) recognized that a plot of D -values vs. ionic radius for a given valence and crystallographic site resulted in a parabolic trend. Blundy and Wood (1994), the first researchers to develop a thermodynamically rigorous predictive model to describe partitioning between crystals and melt, applied lattice strain theory derived by Brice (1975) to rationalize the parabolic

trends observed by Onuma et al. (1968) to form the *lattice strain* model where the equation:

$$D_i = D_0 \times \exp \left[\frac{-4\pi EN \left[\frac{r_0}{2}(r_i - r_0)^2 + \frac{1}{3}(r_i - r_0)^3 \right]}{RT} \right] \quad (1)$$

is used to describe partitioning. D_i is the partition coefficient of element i , D_0 is the coefficient for an element with “ideal” radius r_0 (taken to be the size of a partitioning cation that does not strain the crystal lattice), N is Avogadro's number, E is apparent Young's modulus linked to the compressibility of the site, and r_i is the ionic radius of element i . The model of Blundy and Wood (1994) is advantageous as it can be used to develop predictive relationships for D -values of unstudied or difficult to measure elements provided physio-chemical controls on E , D_0 , and r_0 can be quantified. When the D -values of a few isovalent cations, for example 3+ cations, are plotted against their ionic radii, the D -values for all other elements with the same charge that partition into the same crystallographic site, can be calculated from the resulting parabola. Accordingly, when the lattice strain model prevails, the maximum of the parabola corresponds to D_0 with an associated ionic radius of r_0 , and the width of the parabola corresponds to $1/E$ (Fig. 1). Values for D_0 , r_0 , and E can easily be determined by fitting measured D_i values to Equation 1. Hence, knowing these values in turn allows one to calculate

* E-mail: dwarzski@unm.edu

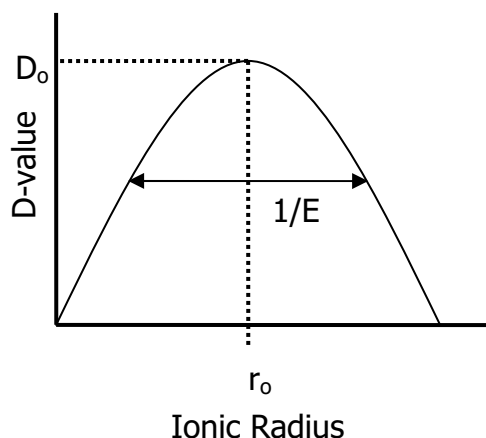


FIGURE 1. Diagram of essential parameters for the lattice strain model.

D_i for any isoivalent trace-element cation partitioning into that site. In the case of garnet, D_0 , r_0 , and E have been shown to vary systematically with mineral composition, temperature, pressure, and crystal site (van Westrenen et al. 1999, 2000, 2001b). Our understanding of these interrelationships is incomplete, however, and this study was designed in part to help further that understanding.

From Blundy and Wood's (1994) lattice strain model, van Westrenen et al. (2001b) developed a predictive relationship to describe partitioning between garnet and silicate melt for trivalent cations entering the garnet X-site. They did this by parameterizing fits of experimental data to Equation 1, which yielded values for D_0 , r_0 , and E , against temperature, pressure, garnet major element composition, and garnet-melt D_{Mg} . Van Westrenen et al.'s model was found to predict successfully D -values between garnet and melt for REE, Sc, and Y to within 5–50% of the experimentally measured D -values. However, thus far this model has been applied only to 3+ cations partitioning into the garnet X-site in Mg-rich systems appropriate for terrestrial petrogenetic processes. In addition, at its inception, the validity of this model at higher pressures could not be tested due to the absence of experimental data beyond 5 GPa.

Current data on high-pressure (>3.5 GPa) partitioning of trace elements into garnet are sparse and almost no data exist on garnet partitioning at high pressure in Fe-rich bulk compositions (Draper et al. 2003). Most studies have focused on predominantly magnesian compositions, relevant to the Earth's upper mantle, at pressures up to 3.4 GPa (e.g., Nicholls and Harris 1980; Salters and Longhi 1999; Salters et al. 2002). Exceptions include studies by Draper et al. (2003, 2004, 2006), Corgne and Wood (2004), Walter et al. (2004), Dworzski and Draper (2004), and Dworzski et al. (2005a, 2005b). Draper et al. (2003) presented partitioning data from an Fe-rich chondritic bulk composition for trace-element partitioning from 5–9 GPa. Corgne and Wood (2004) published a trace-element partitioning study at 25 GPa for majoritic garnets. Draper et al. (2004, 2006) investigated garnet-melt partitioning in a low-Ti, Fe-rich lunar picritic glass composition. Finally, preliminary results have been reported by Dworzski and Draper (2004) and

Dworzski et al. (2005a, 2005b) on trace-element partitioning between garnet and melt in a high Ti, Fe-rich lunar picrite composition. All of these studies demonstrate that the lattice strain model can be used to describe partitioning, but the predictive model of van Westrenen et al. (2001b) does not fully account for trace-element partitioning between garnet and melt in these Fe-rich bulk compositions.

The goals of this study were to evaluate the effect of Ti, Cr, and majorite component on near-liquidus garnet-melt trace-element partitioning in an Fe-rich system. Owing to its high Fe and Ti contents, the Apollo 14 black glass composition was chosen to investigate what effect these elements may have on garnet-melt partitioning at high pressures. Furthermore, the work presented here is part of a larger study to acquire data necessary to extend the predictive relationship of van Westrenen et al. (2001b) to virtually all natural magmatic garnet compositions. These include garnets grown from Fe-rich liquids, as well as those having a substantial majorite component. These varieties of garnet compositions are important for understanding extraterrestrial petrogenesis, in addition to sharpening constraints on terrestrial magmatism.

EXPERIMENTAL AND ANALYTICAL TECHNIQUES

High-pressure experiments

Starting materials. Two variations of the Apollo 14 black glass composition were used as starting material (Table 1). The first was a synthetic analog of the Apollo 14 black (A14B) composition made from analytical grade oxides and then melted to a glass-like quench consisting of numerous micro-crystals (such ultramafic compositions are difficult to quench to glass). This glassy material was ground into a fine powder with an agate mortar and pestle. The second starting composition (A14B-no Cr) was also a synthetic analog of Apollo 14 black glass, but without Cr or alkali oxides. The A14B-no Cr was prepared as a mechanical mixture of analytical grade oxides.

Both starting compositions were doped with a suite of trace elements (Sc, Sr, Y, Zr, Ba, Nd, Sm, Dy, Yb, Hf, and Th) at approximately 200–300 times chondritic abundances to ensure that their concentrations would be well above the detection limit of the ion microprobe, but present in low enough abundance that Henry's Law prevails (see Table 1 for trace-element concentrations). The doping process entailed mechanically mixing an acid solution containing these trace elements into the starting powders. After the solvent evaporated, the mixture was again ground with an agate mortar and pestle under ethanol to promote homogeneity. All starting materials were stored in a desiccator between experiments.

Although the same doping procedure was followed for both starting compositions, the Zr and Hf abundances in A14B-no Cr are almost an order of magnitude higher than those in A14B. This results from Zr and Hf being relatively insoluble in the acid solution (precipitating out of solution) and therefore heterogeneous amounts of those trace elements were added to the starting materials. Hence, Zr is not present in trace amounts in the A14B-no Cr starting composition.

Experimental conditions. Experiments were run in a Walker-style 2000-ton hydraulic multi-anvil press located in the High-Pressure Experimental Petrology Lab at the University of New Mexico (UNM). Experiments were performed under nominally anhydrous conditions at pressures between 3.0 to 7.0 GPa, and temperatures ranging from 1550–1850 °C (Table 2). The experimental cell used was designed and described by Agee et al. (1995). Cast, fanned octahedra of Aremco Ceramacast 584 were used as the pressure medium for all experiments. Graphite capsules were filled with starting material and sealed with press-fit lids. A W5Re-W26Re thermocouple was inserted radially through drilled octahedra fins, so that it made contact with the rhenium foil heater near the centrally positioned capsule. No correction was applied for the effect of pressure on thermocouple emf. The octahedron was then placed within a set of tungsten carbide cubes (either from Kennametal or Fansteel), with corners truncated to 8 mm edge length (TEL).

Pressures for this 8 mm TEL cell were calibrated against the 3 GPa/1000 °C quartz-coesite and the 9 GPa/1200 °C coesite-stishovite phase transitions.

TABLE 1. Starting materials*

	A14B				Trace elements			
	Delano (1986)	A14B (A90)†	A14B—No Cr (A133)†		A14B (A96)	S.D.	A14B-no Cr (A133)	S.D.
SiO ₂	34.00	31.30	36.00	Sc	3503	68	2575	59
TiO ₂	16.40	20.70	14.10	Sr	1801	282	3126	236
Al ₂ O ₃	4.60	5.00	5.50	Y	702	38	706	33
FeO	24.50	24.50	24.00	Zr	2280	62	27578	488
MnO	0.31	0.00	0.30	Ba	662	85	795	36
MgO	13.30	11.90	14.40	Nd	142	10	146	5
CaO	6.90	5.30	5.60	Sm	62	5	62	4
Na ₂ O	0.23	0.10	n.d.	Dy	85	6	83	4
K ₂ O	0.16	0.20	n.d.	Yb	71	3	72	4
P ₂ O ₅	n.a.	n.d.	n.d.	Hf	63	3	521	25
Cr ₂ O ₃	0.92	1.10	n.d.	Th	13	1	13	1
Total	101.32	100.00	100.00					

* Major element data given in weight percent (wt%). Trace element data given in parts per million (ppm).

† Experiments A90 and A133 analyses totals normalized to 100%, to eradicate low totals resulting from quench texture and carbon dissolution into quench.

TABLE 2. Run table

Run	Temperature (°C)	Pressure (GPa)	Duration (min)	Composition	Assemblage
A115	1600	3.0	7	A14B, no Cr	Liquid (100)
A133	1650	3.0	23	A14B, no Cr	Liquid (100)
A105	1600	3.5	47	A14B	Liquid (100)
A158	1575	4.0	13	A14B	Liquid (86), garnet (10)
A156	1800/1600*	4.0	18	A14B	Liquid (100)
A162	1600	5.0	21	A14B	Liquid (76), garnet (19)
A160	1650	5.0	24	A14B	Liquid (83), garnet (13)
A80	1850	5.5	182	A14B	Liquid (100)
A82	1750	5.5	32	A14B	Liquid (100)
A85	1650	5.5	135	A14B	Liquid (61), garnet (36), rutile (5)
A90	1800/1675*	5.5	165	A14B	Liquid (100)
A96	1800/1660*	5.5	120	A14B	Liquid (100)
A97	1675	5.5	60	A14B	Liquid (91), garnet (9)
A98	1660	5.5	64	A14B	Liquid (98), garnet (4)
A161	1800/1670*	5.5	25	A14B, no Cr	Liquid (72), garnet (23), pyroxene (5)
A119	1700	6.3	2	A14B	Liquid (91), garnet (8)
A103	1650	7.0	60	A14B	Liquid (93), garnet (7)
A120	1700	7.0	47	A14B	Liquid (100)
A129	1675	7.0	7	A14B	Liquid (100)
A132	1650	7.0	28	A14B	Liquid (85), garnet (15)
A134	1625	7.0	34	A14B	Liquid (88), garnet (13)

* Two temperatures listed for an experiment indicates a super-liquidus step was employed.

Experiments were pressurized (at a rate of 5 GPa/h) and heated simultaneously to target conditions, then held at those conditions for the duration of the experiment. Experiments were quenched by first cutting the electrical power to the heater and then decompressing for approximately 12 hours. The multi-anvil was not water-cooled during any experiment. Products of successful experiments were mounted in epoxy and polished for electron- and ion-microprobe analysis after removal from the press.

Establishing equilibrium in multi-anvil experiments can be challenging, as large thermal gradients typically are present in experimental cells. The following attempts were made to ensure that equilibrium was closely approached in our experiments. First, graphite capsules of a length designed to position the sample properly in the “hot-spot” of the heater (~2.7 mm) were used to minimize temperature gradients in the 8 mm TEL assembly. Second, the well-formed euhedral garnets were homogenous, verified by consistent gray-scale values in back-scattered electron (BSE) images from the electron probe microanalyzer (EPMA) and by quantitative EPMA analyses. Least-squares mass balances were calculated and the quality of these calculations was assessed by the resulting sum of the square of the residuals (Σr^2) between the known starting composition and that resulting from the mass balance. Next, garnets had values of K_D [= (FeO^{garnet}MgO^{liquid})/(MgO^{garnet}FeO^{liquid})] values ranging from 0.31–0.50, which are consistent with those determined in several other studies (e.g., Yurimoto and Ohtani 1992; Agee et al. 1995; Herzberg and Zhang 1996; van Westrenen et al. 2000; Draper et al. 2003). Finally, there is no significant difference in garnet K_D values for experiments of different durations (Fig. 2); therefore, we infer that equilibrium was approached to an acceptably close extent in these high-pressure experiments.

Analytical techniques

Electron microprobe analyses. All experimental run products were analyzed for major elements on a JEOL 8200 EPMA at UNM. A beam current of 20 nA with an accelerating potential of 15 keV was used for all analyses. Crystals were

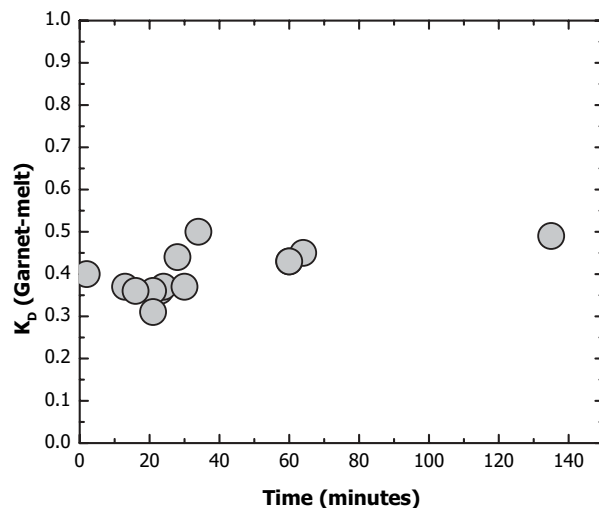


FIGURE 2. Plot of garnet-melt K_D value [$K_D = (\text{FeO}^{\text{garnet}}\text{MgO}^{\text{liquid}})/(\text{MgO}^{\text{garnet}}\text{FeO}^{\text{liquid}})$] vs. time for all garnet-bearing experiments. Similarity of K_D values indicate that experiments approached equilibrium conditions.

analyzed with a focused beam of approximately 1 μm diameter, and a 20 μm “broad” beam was used to analyze quench material that, like the starting material itself, does not quench to glass. Use of a broad beam averages regions of quenched liquid that are highly microcrystalline. Counting times were generally 20–30 sec-

onds on peak and 10–15 seconds on background. The analytical routine consisted of calibrating the EPMA with a fixed beam using natural and synthetic mineral standards. Microprobe data were reduced with online ZAF correction procedures. To ensure analysis quality, a well-characterized pyrope standard was measured as an “unknown” and the results compare well in-house documented compositions. The standard deviations of each pyrope standard measurement from every analytical session are shown in Table 3.

As indicated above, it is very difficult to quench an ultramafic composition to a glass, especially at high pressure (e.g., Ohtani et al. 1989), and our experiments confirm this difficulty. The melt phase in these experimental run products is a textured intergrowth of many microcrystallites and glass. Due to the quench texture, it was almost impossible to obtain EPMA analyses that total 100%; instead, analyses yielded totals ranging from 90.05 to 98.13 wt%. Garnet totals averaged 100 wt%; therefore, we believe that the calibration was acceptable and the low totals were specific to quench analyses.

Secondary ion mass spectrometer analyses. Trace elements were analyzed on a Cameca 4f secondary ion mass spectrometer (SIMS) at UNM. After EPMA analyses, the carbon coats were removed from the experimental run products. The charges subsequently were cleaned using ethyl alcohol, and then gold coats ~15.0 nm thicknesses were applied for SIMS analysis. All run products were analyzed with a primary beam of O⁻ ions having a spot size of 15–20 μm. The primary beam was accelerated through a potential of 10 keV, with a primary current of 20 nA. Secondary ions were energy filtered using an energy window of ±25 V and an offset voltage of 105 V. Element intensities were measured by repeated cycles of peak counting. The trace-element concentrations in the doped samples exceeded the expected detection limits of most elements (<100 ppb). Ion imaging was used to distinguish between crystals and glass before any analyses were performed. To measure trace elements in an experimental run product, the following isotopes were monitored: ³⁰Si, ⁴⁵Sc, ⁸⁸Sr, ⁸⁹Y, ⁹⁰Zr, ¹³⁸Ba, ¹⁴²Nd, ¹⁴⁷Sm, ¹⁶³Dy, ¹⁷⁴Yb, ¹⁸⁰Hf, and ²³²Th. Mass 18.7 or 22.7 was examined during each set of analyses to monitor and correct for background noise.

The daily SIMS calibration curves were constructed from 3 or 4 glass standards for each element, and calibrations were assessed by the linearity of fits of the ³⁰Si-normalized element intensity [(TE/³⁰Si) × SiO₂ wt%], where TE is the trace element of interest] against its concentration. All elements thus plotted had correlation coef-

ficients (*r*²) above 0.97. To further ensure accurate calibrations, a well-characterized standard, NBS 610 (Pearce et al. 1997), was measured as an “unknown” during each analytical session and the results compared well with published compositions. The standard deviations from measurements of every analytical session are shown in Table 4. Absolute concentrations of each element were calculated from the empirical relationships derived from the daily calibration curves.

After SIMS analysis, the gold coats were removed from the run products, which were then checked optically to verify that the SIMS pits occurred at expected places on samples, i.e., directly on a crystal or glass. Plots of ³⁰Si-normalized element intensity against measurement cycle were used to assess whether the SIMS beam sampled small melt inclusions in the crystal or the underlying glass (i.e., an increase in incompatible element concentration with increasing measurement cycle). Ion imaging was employed to ensure that no visible melt inclusions were analyzed by the SIMS beam. Finally, the anomalously large contents of highly incompatible elements characteristic of melt inclusions were absent from the data set.

RESULTS

Major elements

Experimental run products from A14B consisted predominantly of garnet with sizes ranging from 5 to 150 μm surrounded by quench material (Figs. 3 and 4). A few experiments, which were ~50 °C below the liquidus, also contained rutile and low-Ca pyroxene. The garnets grown from this Ti-rich lunar composition have distinct major-element compositions (Table 3) that range from Py₅₀Alm₃₉Gr₁₁ to Py₆₅Alm₂₈Gr₇ where mol% pyrope = $\frac{Mg}{Ca+Fe+Mg} \times 100$, and mol% almandine = $\frac{Fe}{Ca+Fe+Mg} \times 100$, and mol% grossular = $\frac{Ca}{Ca+Fe+Mg} \times 100$. No majorite component was found in any of the garnets grown from the A14B composition.

TABLE 3. Mineral and melt EPMA analyses*†

	A158				A162				A160			
	Quench	S.D.	Garnet	S.D.	Quench	S.D.	Garnet	S.D.	Quench	S.D.	Garnet	S.D.
SiO ₂	28.90	0.30	41.19	0.34	28.04	0.46	41.12	0.60	28.60	0.64	39.73	0.57
TiO ₂	22.93	0.31	2.22	0.07	25.28	0.49	2.59	0.36	23.42	0.79	2.44	0.50
Al ₂ O ₃	4.14	0.32	16.79	0.17	2.10	0.11	16.22	0.93	3.41	0.11	16.51	0.32
FeO	23.70	0.19	14.12	0.11	25.02	0.29	15.38	0.48	24.08	0.40	14.87	0.32
MnO	0.01	0.01	0.02	0.02	0.01	0.01	0.02	0.01	0.01	0.01	0.03	0.02
MgO	11.65	0.22	18.77	0.17	10.68	0.17	18.18	0.70	11.17	0.32	18.37	0.40
CaO	4.40	0.29	2.70	0.09	4.85	0.22	3.20	0.45	4.63	0.48	2.91	0.26
Na ₂ O	0.02	0.02	0.00	0.01	0.04	0.02	0.00	0.00	0.02	0.02	0.00	0.01
K ₂ O	0.13	0.03	0.00	0.00	0.07	0.03	0.00	0.00	0.14	0.05	0.00	0.00
P ₂ O ₅	0.01	0.01	0.00	0.00	0.01	0.00	0.00	0.00	0.01	0.01	0.00	0.00
Cr ₂ O ₃	1.12	0.04	5.78	0.23	0.68	0.03	4.08	0.51	0.96	0.04	4.70	0.34
Total	97.02	0.45	101.59	0.14	96.78	0.55	100.79	0.68	96.46	1.57	99.58	0.63
Fe/Mg K _D			0.37				0.36				0.37	
X _{Mg}	46.7		70.3		43.2		67.8		45.3		68.8	
D _{Ti}			0.10				0.10				0.10	
D _{Cr}			5.14				5.97				4.88	

	A97				A98				A119			
	Quench	S.D.	Garnet	S.D.	Quench	S.D.	Garnet	S.D.	Quench	S.D.	Garnet	S.D.
SiO ₂	28.51	0.75	40.73	0.21	28.17	2.03	40.58	0.33	29.45	0.72	41.54	0.17
TiO ₂	21.21	0.72	1.79	0.21	19.72	0.93	1.38	0.13	21.57	0.50	2.26	0.26
Al ₂ O ₃	3.05	0.17	17.14	0.36	3.92	0.43	17.96	0.36	3.75	0.38	16.94	0.52
FeO	23.53	0.25	16.11	0.13	22.74	0.30	16.16	0.09	24.35	0.35	16.16	0.28
MnO	0.01	0.01	0.02	0.01	0.01	0.01	0.01	0.01	0.01	0.01	0.02	0.01
MgO	10.76	0.26	17.07	0.11	10.64	0.40	16.92	0.16	10.76	0.17	17.62	0.17
CaO	5.08	0.31	3.10	0.06	5.06	0.27	2.67	0.06	5.22	0.35	3.72	0.17
Na ₂ O	0.04	0.02	0.01	0.01	0.04	0.03	0.02	0.03	0.03	0.02	0.00	0.02
K ₂ O	0.04	0.01	0.00	0.00	0.04	0.01	0.01	0.01	0.06	0.02	0.00	0.00
P ₂ O ₅	0.02	0.01	0.00	0.00	0.02	0.01	0.00	0.00	0.02	0.01	0.00	0.01
Cr ₂ O ₃	0.86	0.04	3.71	0.09	0.92	0.09	3.63	0.22	0.90	0.03	3.77	0.10
Total	93.12	1.21	99.69	0.39	91.28	2.40	99.35	0.59	96.11	0.50	102.02	0.27
Fe/Mg K _D			0.43				0.45				0.40	
X _{Mg}	44.9		65.4		45.5		65.1		44.1		66.5	
D _{Ti}			0.08				0.07				0.10	
D _{Cr}			4.30				3.93				4.20	

TABLE 3.—Continued

	A85						A103			
	Quench	S.D.	Garnet	S.D.	Ilmenite	S.D.	Quench	S.D.	Garnet	S.D.
SiO ₂	24.18	1.70	39.43	0.51	0.48	0.01	29.01	0.67	41.31	0.30
TiO ₂	22.45	1.31	3.13	0.67	92.56	0.46	21.08	0.53	1.58	0.12
Al ₂ O ₃	0.91	0.31	14.23	1.38	0.52	0.06	3.31	0.29	17.77	0.17
FeO	26.72	0.41	20.17	0.48	2.74	0.09	23.49	0.31	16.22	0.11
MnO	0.01	0.01	0.02	0.02	0.01	0.01	0.01	0.01	0.02	0.02
MgO	9.46	0.47	14.73	0.57	0.19	0.02	10.76	0.51	17.39	0.08
CaO	5.93	0.39	4.66	0.44	0.15	0.03	5.46	0.50	3.10	0.06
Na ₂ O	0.04	0.03	0.01	0.02	0.00	0.01	0.04	0.02	0.01	0.01
K ₂ O	0.03	0.01	0.00	0.00	0.00	0.00	0.02	0.01	0.00	0.00
P ₂ O ₅	0.02	0.01	0.00	0.00	0.00	0.00	0.01	0.01	0.00	0.01
Cr ₂ O ₃	0.29	0.07	3.52	0.28	1.81	0.05	0.92	0.04	3.94	0.08
Total	90.05	1.85	99.90	0.73	98.47	0.34	94.09	0.89	101.35	0.33
Fe/Mg K _D			0.49						0.43	
X _{Mg}	38.7		56.5				44.9		65.6	
D _{Ti}			0.14		4.12				0.08	
D _{Cr}			12.12		6.23				4.30	

	A161						A132			
	Quench	S.D.	Garnet	S.D.	Opx	S.D.	Quench	S.D.	Garnet	S.D.
SiO ₂	30.81	0.27	41.67	0.30	55.34	0.64	27.74	0.38	40.59	0.22
TiO ₂	17.10	0.42	3.45	0.49	0.31	0.02	22.79	0.42	2.00	0.20
Al ₂ O ₃	1.88	0.12	16.53	0.80	0.70	0.10	2.14	0.11	16.84	0.75
FeO	27.62	0.18	16.44	0.66	15.19	0.15	23.89	0.12	17.09	0.26
MnO	0.37	0.02	0.42	0.02	0.26	0.02	0.00	0.01	0.02	0.02
MgO	11.31	0.16	18.34	0.36	27.62	0.30	10.33	0.29	16.69	0.36
CaO	5.01	0.34	3.53	0.23	1.47	0.06	5.46	0.20	3.44	0.42
Na ₂ O	0.01	0.02	0.00	0.01	0.02	0.01	0.03	0.02	0.01	0.01
K ₂ O	0.02	0.01	0.00	0.00	0.00	0.00	0.09	0.01	0.00	0.00
P ₂ O ₅	0.03	0.01	0.01	0.01	0.00	0.00	0.01	0.01	0.00	0.00
Cr ₂ O ₃	0.00	0.00	0.01	0.01	0.00	0.01	0.62	0.03	3.76	0.44
Total	94.15	0.28	100.41	0.31	100.91	0.68	93.10	0.59	100.44	0.31
Fe/Mg K _D			0.35		0.21				0.44	
X _{Mg}	42.2		66.5		76.4		43.5		63.5	
D _{Ti}			0.20		0.02				0.09	
D _{Cr}									6.06	

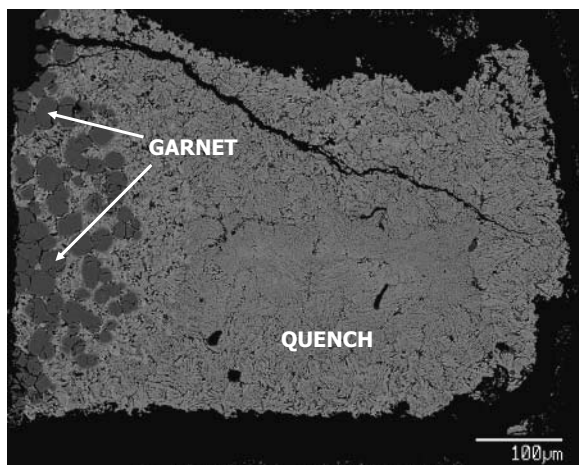


FIGURE 3. Back-scattered electron image of experiment A103 run product showing garnet crystals surrounded by quenched melt. Textured quench was present in all experimental run products.

However, the garnets grown did contain up to 3 wt% TiO₂ and had large Cr contents, reaching almost 6 wt% Cr₂O₃.

Upon calculating the garnet formulae and assigning cations to the X- and Y-sites in the traditional way, the garnet stoichiometry did not balance. For the pyrope garnet structure, the X-site should have 3 cations, but $\Sigma[\text{Mg}^{2+} + \text{Fe}^{2+} + \text{Ca}^{2+} + \text{Mn}^{2+}]$ resulted in totals

TABLE 3.—Continued

	Pyrope Standard				
	Measured	Known	S.D.	Percent Error (%)	Absolute Error (\pm wt%)
SiO ₂	42.21	42.26	0.25	0.12	0.05
TiO ₂	0.50	0.49	0.04	1.25	0.01
Al ₂ O ₃	21.73	21.75	0.32	0.11	0.02
FeO	8.44	8.51	0.14	0.82	0.07
MnO	0.31	0.33	0.04	5.03	0.02
MgO	21.08	20.91	0.11	0.81	0.17
CaO	4.20	4.25	0.22	1.08	0.05
Cr ₂ O ₃	1.81	1.84	0.04	1.44	0.03
Total	100.28	100.34			

* All analyses given in wt%.

† For major element analyses, S.D. is standard deviation of measurement.

‡ For pyrope standard analyses, S.D. is standard deviation of 15 analytical sessions on the EPMA from 8/5/2004 to 3/29/2005.

greater than 3 (3.1 to 3.36 per formula unit). Similarly, the Y-site should hold 2 cations per formula unit, but generally had less than 2 (1.63 to 1.89 per formula unit), calculated as $\Sigma[\text{Al}^{3+} + \text{Cr}^{3+} + \text{Ti}^{4+}]$. These site assignments assume that all Fe is present in Fe²⁺ form. We address these stoichiometric assignments in detail in the Discussion section.

In terms of garnet end-members, garnet compositions from the Cr-free starting material (A14B-no Cr) range from Py₅₆Alm₃₄Gr₉ to Py₆₂Alm₃₀Gr₈, and have 2.4–3.4 wt% TiO₂. These compositions are very similar to the major-element compositions of garnets grown from A14B. The formulae for these garnets similarly shows excess X-site cations and deficient Y-site cations. Interestingly, there is a slight majorite signature in garnets

TABLE 4. Trace element abundances (in ppm) and garnet-melt partition coefficients*†

	A85						A119					
	Garnet	S.D.	Quench	S.D.	<i>D</i>	σD	Garnet	S.D.	Quench	S.D.	<i>D</i>	σD
Sc	4717	235	1894	79	2.49	0.16	4659	208	3056	17	1.52	0.07
Sr	347	219	1849	244	0.19	0.12	64	7	1632	202	0.04	0.01
Y	781	14	601	48	1.30	0.11	490	59	663	9	0.74	0.09
Zr	931	343	3158	368	0.29	0.11	271	76	2221	13	0.12	0.03
Ba	64	38	396	112	0.16	0.11	18	4	549	77	0.03	0.01
Nd	27	6	136	20	0.20	0.06	7	1	129	4	0.05	0.01
Sm	22	2	53	7	0.42	0.07	6	2	55	2	0.12	0.03
Dy	74	4	88	5	0.84	0.06	41	9	84	2	0.48	0.10
Yb	113	1	50	6	2.26	0.27	94	2	66	2	1.41	0.06
Hf	31	8	79	10	0.39	0.11	11	3	61	1	0.18	0.04
Th	5	1	15	2	0.34	0.06	1	0	11	0	0.10	0.02

	A161						A103					
	Garnet	S.D.	Quench	S.D.	<i>D</i>	σD	Garnet	S.D.	Quench	S.D.	<i>D</i>	σD
Sc	3924	62	1933	20	2.03	0.04	4028	149	3093	65	1.30	0.06
Sr	22	9	1688	213	0.01	0.01	106	25	1323	58	0.08	0.02
Y	686	45	655	21	1.05	0.08	327	25	601	28	0.54	0.05
Zr	5938	594	33055	428	0.18	0.02	229	29	2435	47	0.09	0.01
Ba	2	2	458	23	0.004	0.004	39	22	401	47	0.10	0.06
Nd	7	1	171	11	0.04	0.01	7	1	111	6	0.06	0.01
Sm	10	1	70	3	0.14	0.02	8	2	55	4	0.14	0.04
Dy	63	6	96	4	0.66	0.07	28	1	83	5	0.34	0.02
Yb	108	5	61	2	1.78	0.09	72	8	67	4	1.07	0.14
Hf	142	15	586	0	0.24	0.03	13	1	62	2	0.21	0.02
Th	1	0	14	1	0.04	0.01	2	0	10	2	0.21	0.04

	NBS 610‡		
	Measured	Standard	S.D.
Sc	441	441	0.3
Sr	538	516	20.5
Y	450	450	0.2
Zr	445	440	3.8
Ba	429	424	4.8
Nd	431	431	0.1
Sm	450	451	0.0
Dy	426	427	0.0
Yb	461	462	0.0
Hf	418	418	0.0
Th	457	457	0.0

* Abundances given in parts per million (ppm).

† *D*-values listed are from ratios of SIMS ³⁰Si-normalized element intensities. σD is the calculated uncertainty propagated from standard deviations of SIMS analyses using $\sigma D = D \sqrt{\left(\frac{\sigma_A}{A}\right)^2 + \left(\frac{\sigma_B}{B}\right)^2}$. $D = (A \pm \sigma_A) / (B \pm \sigma_B)$ where *A* is concentration (ppm) of the trace element in the garnet with a standard deviation of σ_A , and *B* is the concentration (ppm) of the trace element in the melt with a standard deviation of σ_B .

‡ NBS 610 measured values are average of measurements from 5 different analytical sessions from 8/18/04 to 2/28/05. S.D. is standard deviation from the different analytical sessions.

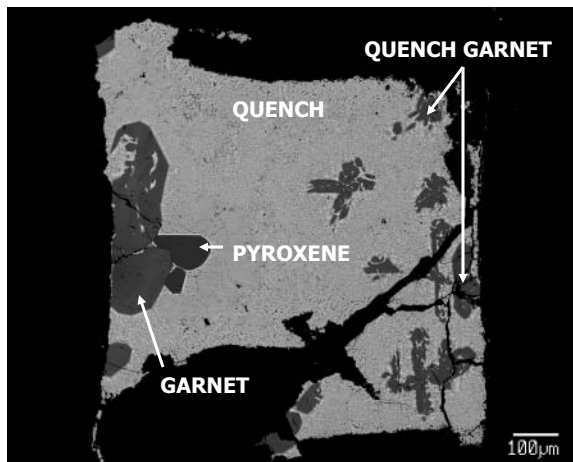


FIGURE 4. Back-scattered electron image of experiment A161 run product from the Cr-free starting material showing large garnet in equilibrium with pyroxene, quench garnets, and quenched liquid.

grown in experiment A161, at 5.5 GPa, shown by 3.07 Si per formula unit.

Trace-element partitioning

Table 4 lists trace-element concentrations measured in garnet and glass on the SIMS. *D*-values listed there are from the intensity ratios measured on the SIMS. Comparisons with literature *D*-values are shown in Figure 5 for the 3+ and 4+ cations.

Garnet-melt partition coefficients for Ti and Cr in compositions A14B and A14B-no Cr are shown in Table 3. Although Ti and Cr were present in the initial starting powders as major and minor elements, respectively, it is nonetheless worthwhile to examine how they partition into garnet. Titanium behaves incompatibly in these garnets, with measured D_{Ti} values ranging from 0.07 to 0.14 in A14B, and 0.12 to 0.20 in the A14B-no Cr composition. The slightly higher *D*-values for D_{Ti} in the Cr-free composition indicate that Ti may be more compatible in this composition, probably because it is not competing with Cr³⁺ for the Y-site. Chromium is highly

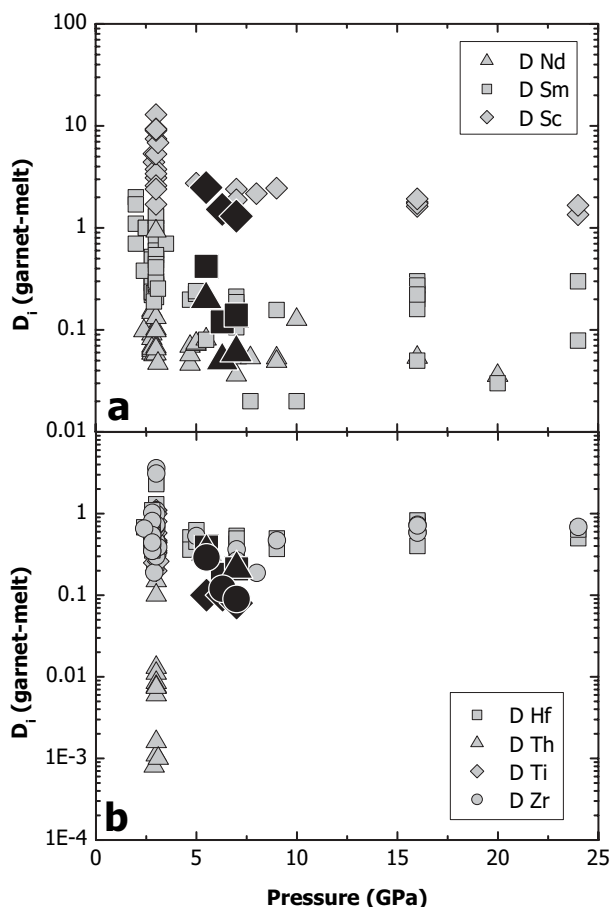


FIGURE 5. Comparison between A14B D -values (in black) with literature values (in gray) from Nicholls and Harris (1980), Kato et al. (1987), Ohtani et al. (1989), Yurimoto and Ohtani (1992), Salters and Longhi (1999), van Westrenen et al. (1999, 2000), Inoue et al. (2000), Draper et al. (2003), and Pertermann et al. (2004). (a) Comparison of 3+ cation (Nd, Sm, and Sc) D -values up to 25 GPa between A14B experiments and literature values. (b) Comparison of 4+ cation D -values with literature values up to 25 GPa.

compatible in garnet from the A14B composition, with D_{Cr} ranging from 3.9 to 12.1.

DISCUSSION

Major elements

The results of stoichiometric calculations presented (Table 5) here are robust and relevant to the following discussion of the A14B and A14B-no Cr garnet crystal chemistry. Errors for the analysis of each element in the standards (shown in Table 3) were propagated through the stoichiometry calculations to verify that the excesses and deficiencies discussed herein are valid. For example, after the stoichiometry for Si was calculated, we took the error obtained from the repeated standard analyses for Si (± 0.05 wt%), carried it through the stoichiometric calculation, and found that for Experiment A85 garnet the Si value was 3.02 ± 0.01 Si per 12 O.

Every garnet stoichiometric calculation for both A14B and A14B-no Cr resulted in excess X-site cations and deficient Y-site cations. The “excess X” is attributed to either Fe (Fe^{3+} or Fe^{2+}) or Mg. We consider two possibilities to explain this observation. Either Fe^{2+} or Mg^{2+} is going into the Y-site to charge balance Ti^{4+} , or Fe^{3+} may indeed be present. However, the presence of Fe^{3+} is unlikely on three accounts. The first, and simplest, is that the graphite capsules used here are thought to impose an oxygen fugacity (f_{O_2}) near that of the iron-wüstite (IW) buffer, and at such conditions only very small amounts of Fe^{3+} would be present. Second, we calculated the ($X_{Fe_2O_3}^{liq}/X_{FeO}^{liq}$) in the experimental liquids assuming a realistic range of f_{O_2} (IW–1 to IW+1) following the procedure of Kilinc et al. (1983), where

$$\ln(X_{Fe_2O_3}^{liq}/X_{FeO}^{liq}) = a \ln f_{O_2} + \frac{b}{T} + c + \sum_i d_i X_i \quad (2)$$

is used to get a rough estimate of the potential amount of Fe^{3+} present in the liquids of run products. The constants a , b , c , and d_i result from multiple linear regressions used by Kilinc et al. to parameterize experimental data. The results of those calculations indicate that garnet Fe^{3+} contents (~ 0.03 wt% Fe_2O_3) are not a significant contribution to the stoichiometry calculation, and therefore Fe^{3+} cannot account for the excess X-site cations. Magmatic garnets, in general, do not have much Fe^{3+} incorporated into their structure; in fact, Fe^{3+} is thought to behave incompatibly in garnets during melting (e.g., Woodland and Koch 2003).

Third and finally, although structural formulae were recalculated for all garnet analyses using the formulation of Droop (1987), which does permit some Fe^{3+} to be present in the garnets, the recalculation of garnet stoichiometry to account for the presence of Fe^{3+} does not solve the excess X or deficient Y issue. The X-site cation sums remain >3 , and the Y-site cation sums are still <2 . The results of the Kilinc and Droop procedures indicate that there is the potential for at least a small amount of Fe^{3+} to be present in the experimental charges, however, not enough to account for the excess X-site cations.

The relative paucity of Fe^{3+} suggests that the excess X cations and deficient Y cations in these Ti- and Cr-rich garnets can be mostly attributed to Fe^{2+} , Mg^{2+} , or both filling the octahedrally coordinated Y-site to charge balance with Ti^{4+} . Although Ti^{4+} is incompatible in these garnets, the extreme amount of TiO_2 in this bulk composition results in significant Ti uptake into the garnet structure. The coupled substitution for a 2^+ cation and Ti^{4+} partitioning into the Y-site is described by the following relationship, where R^{2+} is either Mg^{2+} or Fe^{2+} and R^{3+} is Al^{3+} :



It may be more likely that Mg^{2+} would partition into the Y-site because it has a smaller ionic radius than does Fe^{2+} and hence would fit more easily into Y. However, assignment of the “excess X” cations in the form of Mg^{2+} to the Y-site does not charge balance with the Ti^{4+} . Therefore, Si^{4+} is also required to partition onto the Y-site in the following exchange:



Furthermore, as mentioned above, the addition of Si^{4+} on the

TABLE 5. Garnet stoichiometry

	A158	A162	A160	A85	A97	A161
X-site						
Fe	0.86	0.95	0.93	1.29	1.00	1.01
Mn	0.00	0.00	0.00	0.00	0.00	0.03
Mg	1.93	1.80	1.84	1.32	1.74	1.68
Ca	0.21	0.25	0.23	0.38	0.25	0.28
Cation Sum	3.00	3.00	3.00	3.00	3.00	3.00
Bulk Charge	5.99	6.01	6.01	5.99	5.99	6.00
Y-site						
Mg	0.11	0.19	0.20	0.36	0.15	0.33
Ti	0.12	0.14	0.14	0.18	0.10	0.19
Al	1.42	1.39	1.39	1.22	1.48	1.39
Cr	0.33	0.24	0.28	0.21	0.22	0.00
Si	0.02	0.04	0.01	0.06	0.05	0.10
Cation Sum	2.00	2.00	2.02	2.04	2.00	2.02
Bulk Charge	6.04	5.99	6.00	5.99	6.01	6.01
Z-site						
Si	2.98	2.99	2.95	2.96	2.98	2.97
Al	0.02	0.02	0.06	0.06	0.02	0.04
Cation Sum	3.00	3.01	3.01	3.02	3.00	3.01
Bulk Charge	11.97	12.00	11.99	12.02	11.99	11.99
Sum	8.00	8.01	8.04	8.05	8.00	8.02
Py	65.5	62.4	63.7	50.1	60.2	60.5
Alm	27.7	29.6	29.0	38.5	31.9	30.4
Gr	6.8	7.9	7.3	11.4	7.8	8.4
	A98	A119	A103	A132	A134	
X-site						
Fe	1.01	0.97	0.99	1.06	1.18	
Mn	0.00	0.00	0.00	0.00	0.00	
Mg	1.78	1.75	1.77	1.66	1.54	
Ca	0.21	0.29	0.24	0.27	0.29	
Cation Sum	3.00	3.00	3.00	3.00	3.00	
Bulk Charge	6.01	6.00	6.01	6.00	6.00	
Y-site						
Mg	0.10	0.17	0.13	0.19	0.26	
Ti	0.08	0.12	0.09	0.11	0.14	
Al	1.56	1.46	1.51	1.44	1.36	
Cr	0.21	0.22	0.23	0.22	0.20	
Si	0.04	0.03	0.04	0.06	0.05	
Cation Sum	1.99	2.00	2.00	2.01	2.02	
Bulk Charge	5.99	5.99	5.99	6.02	5.99	
Z-site						
Si	2.99	2.99	2.98	2.96	2.99	
Al	0.02	0.01	0.02	0.04	0.01	
Cation Sum	3.01	3.00	3.00	3.00	3.00	
Bulk Charge	12.00	12.00	12.00	12.02	12.01	
Sum	8.00	8.01	8.01	8.02	8.02	
Py	60.6	60.4	60.5	58.0	55.1	
Alm	32.5	30.5	31.7	33.3	36.1	
Gr	6.9	9.0	7.8	8.6	8.8	

Y-site in turn requires transfer of Al^{3+} from the Y-site to the Z-site to provide correct cation sums as well as bulk charge balance per site (e.g., Meagher 1982).

Interestingly, Equation 4 is a very similar exchange to that of majorite component in garnet, which is manifested by an increase in Si and a decrease in Al per formula unit. All garnets grown in this study have less than 2 Al per 12 O, but do not have more than 3 Si, as would be expected for a majoritic component. The presence of Ti^{4+} in the Y-site may be considered a majorite analog, as it is coupled with less than 2 Al per 12 O. This study is the first to document an effect of Ti to produce a “majorite analog.” The effect also appears in the garnet-melt partitioning data, as outlined in the following section.

Application of the Lattice Strain Model to trace elements

Trivalent cations. Garnet-melt trace-element partition coefficients for 3+ cations for both the A14B and A14B-no Cr compositions were applied to the lattice strain model of Blundy and Wood (1994) and compared with the predictive model of van Westrenen et al. (2001b) (Fig. 6). The solid lines in these figures are fits of the data to Equation 1, and the dashed lines show the results of the predictive relationship of van Westrenen et al. (2001b). A significant mismatch exists between the measured D -values of this study and the theoretical prediction of van Westrenen et al. (2001b). This result is consistent with trace-element partitioning measured by Draper et al. (2003) between garnet and chondritic melt, and Corgne and Wood (2004) between majorite and silicate melt, both of which were also more Fe-rich than terrestrial peridotitic magmas.

Although the D -values from this study form a parabola, this parabola is flatter than predicted by the model of van Westrenen et al. (2001b). This flattening indicates that garnet grown from a high-Ti,Fe composition partitions trace elements differently than garnet grown in a Mg-rich, peridotitic composition, with a diminished ability to fractionate the LREE from the HREE. These changes result in a shallow slope of the parabola's limbs. These observations indicate that these garnets will impart a signature different from the “classical” signature to any melts that are extracted from garnet-bearing regions that may exist within the Moon.

Interestingly, the predicted and actual parabolas for the Cr-free composition are not offset as significantly. In fact, the predicted and calculated values of r_0 from the experimental data are within error of each other. Furthermore, the E -values calculated from the Cr-free A14B (Experiment A161) are significantly different from those calculated for the Cr-bearing A14B (Experiment A85). What this finding suggests is that Cr may influence trace-element partitioning between garnet and melt, at least in the Ti-rich compositions used in this study. Additionally, the coupled substitution of $Ti^{4+} + (Fe^{2+}, Mg^{2+})$ into the Y-site may have a significant effect on trace-element partitioning into these garnet crystals. However, at present we cannot decipher which effect is the most significant.

Tetravalent cations. The tetravalent trace-element cations generally reside in the octahedrally coordinated Y-site of the garnet crystal. Although Th is tetravalent, its ionic radius is too large for the Y-site so it prefers the X-site; hence, it is not considered further. No majorite signature was present in any garnet grown from A14B; therefore, lacking a D -value for octahedrally coordinated Si ($D^{VI_{Si}}$), the span in ionic radius was not large enough to apply the lattice strain model to the $4+$ cations without knowing, a priori, values for at least one lattice-strain fit parameter. In addition, estimates of $D^{VI_{Si}}$ only can be minimum values, as not all Si in the melt is in octahedral coordination. At a given ^{VI}Si content for garnet, $D^{VI_{Si}}$ increases with decreasing proportions of ^{VI}Si in the melt phase. Garnets in experiment A161, from the A14B-no Cr composition, had a small but noticeable majorite component, expressed by 3.07 Si per formula unit. Application of the lattice strain model to D -values measured in experiment A161 is shown in Figure 7. No predictive relationship currently exists for $4+$ cation trace-element partitioning into the Y-site of garnet. Because estimated $D^{VI_{Si}}$ is a minimum value, calculated

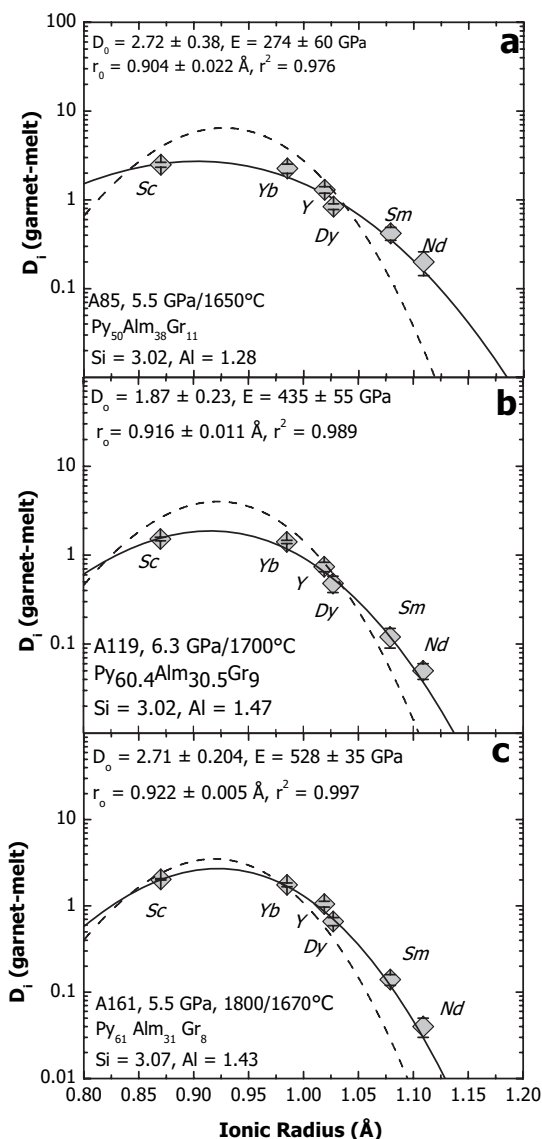


FIGURE 6. Trace-element partitioning parabolas for A14B and A14B-no Cr. Ionic radii from Shannon (1976). Solid lines are fits of data to the lattice strain model of Blundy and Wood (1994), and dashed lines are trends from the predictive model of van Westrenen et al. (2001b). (a) van Westrenen et al. (2001b) predicts $D_0 = 6.45$, $r_0 = 0.928 \text{ \AA}$, and $E = 705 \text{ GPa}$. (b) van Westrenen et al. (2001b) predicts $D_0 = 4$, $r_0 = 0.9224 \text{ \AA}$, and $E = 748 \text{ GPa}$. (c) van Westrenen et al. (2001b) predicts $D_0 = 3.49$, $r_0 = 0.9188 \text{ \AA}$, and $E = 780 \text{ GPa}$.

E is a maximum possible value.

Two different fits to the tetravalent cations are shown in Figure 7. The functional form of the lattice strain model fits the partitioning of Ti, Hf, Zr, and ${}^{\text{VI}}\text{Si}$, shown by the $r^2 = 0.989$. It is worth mentioning that D_0 for these 4+ cations is 0.2315 ± 0.029 , as all the tetravalent cations applied to the lattice strain model have incompatible D -values. The alternative fit is for Ti, Hf, and Zr, which also predicts an incompatible D_0 of 0.4382 . Therefore, for the garnets grown from A14B-no Cr, it is not expected that the high-field-strength elements would be compatible, as docu-

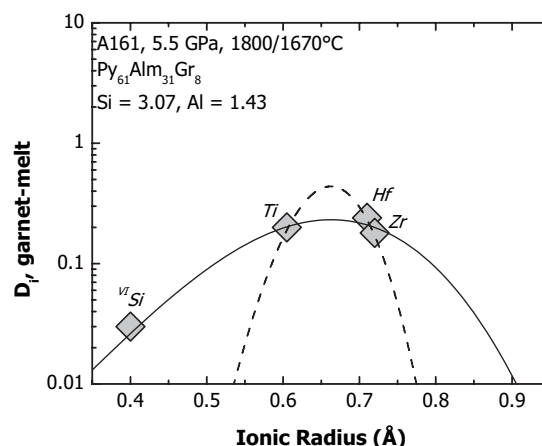


FIGURE 7. Partitioning parabola for 4+ cations in the A14B Cr-free composition. Solid line is fit of data to the lattice strain model of Blundy and Wood (1994), resulting in $D_0 = 0.2315 \pm 0.0285$, $r_0 = 0.6629 \pm 0.0241 \text{ \AA}$, $E = 276 \pm 70 \text{ GPa}$, and $r^2 = 0.989$. The dashed line is a fit to Zr, Hf, and Ti, with $D_0 = 0.4382$, $r_0 = 0.6624 \text{ \AA}$, $E = 1737 \text{ GPa}$, and $r^2 = 1$. Because fit is to 3 data points, uncertainties on fit parameters cannot be calculated and $r^2 = 1$. Error bars on all D -values smaller than size of the symbols.

mented by van Westrenen et al. (2001a). However, the Young's modulus values of the two different fits are significantly different and will be discussed below. Accounting for tetravalent partitioning in garnet is a focus of our ongoing research.

Young's modulus. The garnets grown in this study have some of the lowest apparent Young's modulus values of any garnet crystallographic site calculated using the lattice strain model. It is important at this point to emphasize that these E -values are model dependent. The E -values for the X-site in garnets grown from A14B range from 274 to 435 GPa. The Young's modulus of the X-site for trivalent elements in the Cr-free A14B is 528 GPa. In comparison, van Westrenen et al. (1999) documented E -values ranging from 257 to 590 GPa in garnets grown from a simple system (FCMAS). The E -values published by Pertermann et al. (2004) range from 548 to 800 GPa for the 3+ cations on the garnet X-site. Draper et al. (2003) measured the E -value for the X-site in garnets with a slight majorite component that ranged from 471 to 531 GPa. Similarly, the E -value measured by Corgne and Wood (2004) for a majorite X-site was 521 GPa. Therefore, E -values for the garnet X-site of A14B and A14B-no Cr are low compared with previously measured values.

Two very different solutions to the lattice strain model are possible for the tetravalent cations shown on Figure 7. If Equation 1 is fit including the D for ${}^{\text{VI}}\text{Si}$, a value of $276 \pm 70 \text{ GPa}$ results; if only Ti, Hf, and Zr are used, the resulting value is 1737 GPa (with no associated uncertainty because only three points are being fit). The incorporation of a small majorite component in our garnets took place at lower pressures than in the more magnesian systems studied by most previous authors, in similar fashion to the majorite signature observed by Draper et al. (2003) in an Fe-rich ordinary chondrite composition. Like that study, our bulk composition is significantly more Fe-rich than those studied by previous authors, and, as argued by Draper et al. (2003), majorite incorporation appears to occur at a lower pressure in such

compositions than in more magnesian systems. The tetravalent fit produced by using only Ti, Hf, and Zr yielded $E = 1737$ GPa, which is more similar to values obtained by other authors, such as 1211 to 3273 GPa by van Westrenen et al. (2001a) or 1504 GPa by Corgne and Wood (2004). However, fits obtained using only those three elements, although mathematically defensible, may not be physically realistic because the range of ionic radii for those elements is so small. If, in fact, a D -value for ^{46}Si is meaningful, and octahedral Si resides in garnet's Y-site along with Ti, Hf, and Zr, then E must be much lower (broader parabola) than the high values mentioned above. These considerations suggest that a significant change occurs on the Y-site of the garnet crystal, with compressibility increasing with increasing majorite content. This result may seem counterintuitive because the garnet Y-site is smaller than the X, and smaller size is generally interpreted to correspond to smaller site compressibilities, which in turn should result in higher E values (e.g., Hazen and Finger 1979). However, majorite generally forms with increasing pressure, and with increasing pressure compressibility should decrease.

The low E -values of the garnets grown in this study may be explained in different ways. The first explanation is that there is a significant change to the garnet structure with the incorporation of the high-Ti "majorite analog" component. Also, it is possible that Zr and Hf partition in part into the X-site of the garnets grown in this study. This possibility is consistent with the results of Corgne and Wood (2004) who found that Zr and Hf partition into the X-site in majoritic garnets.

Alternatively, when the trace elements were analyzed in garnets by the SIMS beam, it is possible that quenched melt was included along with garnet. This might occur if melt inclusions were present in the crystal or if glass adjacent to (or beneath) the analyzed garnet was sampled by the ion beam. This would result in artificially higher D -values for the incompatible elements, and slightly lower D -values for the compatible elements, which would in turn result in a broader parabola and ultimately a lower E -value. Although ion imaging was used on the SIMS to ensure that no melt inclusions were analyzed, and BSE images do not show exposed melt inclusions, their presence is not eliminated unequivocally. Therefore, to test this possibility, the lattice strain model was refit to trivalent D -values except D_{Nd} and D_{Sm} , which would be expected to be the least compatible of the trivalent elements used in this work and hence the most susceptible to the influence of any melt inclusions. The E -values calculated (i.e., A119 $E = 697 \pm 168$ GPa) were not within error of those calculated including D_{Nd} and D_{Sm} . This result indicates that despite precautionary steps, D_{Nd} and D_{Sm} were artificially higher due to incorporation of glass. This situation is similar to one outlined for garnet-melt partitioning in a low-Ti composition (Draper et al. 2006).

In any case, E -values calculated for our garnets omitting D_{Nd} and D_{Sm} remain lower than those predicted by the van Westrenen et al. (2001b) model (i.e., A119 $E = 748$ GPa). Therefore, we conclude that the significantly lower E -values of the garnets in this study are not artificial. They may be the result of the high-Fe bulk composition, as well as the high Ti and Cr contents of the crystals. From a crystal-chemical perspective, why would the presence of Ti^{4+} and Cr^{3+} on the Y-site lower the Young's modulus of the garnet crystal for both the X- and Y-sites? Why

does removal of Cr from the starting composition increase the E value for the X-site? Although we are not yet in a position to answer these questions fully, we can consider several options.

Young's modulus is thought to be an indicator of site rigidity. Very rigid sites will "exclude" ions that differ significantly from the site size and have high E -values (Wood and Blundy 2003). Therefore, the very low E -values for the sites of the garnet crystals grown in this study indicate that these garnets have very compressible sites, for both the Cr-bearing and Cr-free compositions. Van Westrenen et al. (2001a) attempted to relate low E values to garnet Ca contents and suggested that garnets with intermediate Ca have anomalously soft structures. Similarly, the low E values calculated for the garnets grown in this study may be the result of the unusual garnet compositions. Ongoing work in our group will study these effects in greater detail.

ACKNOWLEDGMENTS

This work was funded through NSF grant EAR-0337237 awarded to D.S. Draper and NASA Cosmochemistry Grant 13388 to C.B. Agee. We acknowledge Mike Spilde and Jana Berlin for their help with the EPMA analyses, as well as Paul Burger for assistance with SIMS data reduction. This manuscript benefited greatly from reviews by W. van Westrenen and T. Labotka. R.E.D. thanks Jim Papike for many stimulating discussions regarding garnet crystal chemistry.

REFERENCES CITED

- Agee, C.B., Li, J., Shannon, M.C., and Circone, S. (1995) Pressure-temperature phase diagram for the Allende Meteorite. *Journal of Geophysical Research*, 100, 17725–17740.
- Blundy, J. and Wood, B. (1994) Prediction of crystal-melt partition coefficients from elastic moduli. *Nature*, 372, 452–454.
- Brice, J.C. (1975) Some thermodynamic aspects of the growth of strained crystals. *Journal of Crystal Growth*, 28, 249–253.
- Corgne, A. and Wood, B.J. (2004) Trace element partitioning between majoritic garnet and silicate melt at 25 GPa. *Physics of the Earth and Planetary Interiors*, 143–144, 407–419.
- Delano, J.W. (1986) Pristine lunar glasses; criteria, data, and implications. *Proceedings of the 16th Lunar and Planetary Science Conference, Journal of Geophysical Research*, 91, D201–D213.
- Draper, D.S., Xirouchakis, D., and Agee, C.B. (2003) Trace element partitioning between garnet and chondritic melt from 5 to 9 GPa: Implications for the onset of the majorite transition in the Martian mantle. *Physics of the Earth and Planetary Interiors*, 139, 149–169.
- Draper, D.S., duFrane, S.A., and Shearer, C.K. (2004) Preliminary high-pressure phase relations of Apollo 15 Green C glass: Assessment of the role of garnet. *Lunar and Planetary Science Conference XXXV*, Abstract no. 1297.
- Draper, D.S., duFrane, S.A., Shearer, C.K., Dwarzski, R.E., and Agee, C.B. (2006) High-pressure phase equilibria and element partitioning experiments on Apollo 15 green C picritic glass: Implications for the role of garnet in the deep lunar interior. *Geochimica et Cosmochimica Acta*, 70, 2400–2416.
- Droop, G.T.R. (1987) A general equation for estimating Fe^{3+} concentrations in ferromagnesian silicates and oxides from microprobe analyses, using stoichiometric criteria. *Mineralogical Magazine*, 51, 431–435.
- Dwarzski, R.E. and Draper, D.S. (2004) Effect of titanium on REE and HFSE partitioning between garnet and melt. *Eos, Transactions, American Geophysical Union* 85, Fall Meeting Supplement, Abstract no. V41C-1402.
- Dwarzski, R.E., Draper, D.S., Shearer, C.K., and Agee, C.B. (2005a) High-pressure phase relations and trace element partitioning in Apollo 14 black glass. *Lunar and Planetary Science Conference XXXVI*, Abstract no. 1450.
- Dwarzski, R.E., Draper, D.S., Shearer, C.K., and Agee, C.B. (2005b) Crystal chemical controls on garnet partitioning of REE and HFSE. *Goldschmidt Conference, Moscow, Idaho, May 20–25, 2005*, Abstract no. 1934.
- Hazen, R.M. and Finger, L.W. (1979) Bulk modulus-volume relationship for cation-anion polyhedra. *Journal of Geophysical Research*, 84, 6723–6728.
- Herzberg, C. and Zhang, J. (1996) Melting experiments on anhydrous peridotite KLB-1 composition of magmas in the upper mantle and transition zone. *Journal of Geophysical Research*, 101, 8271–8295.
- Inoue, T., Rapp, R.P., Zhang, J., Gasparik, T., Weidner, D.J., and Irifune, T. (2000) Garnet fractionation in a hydrous magma ocean and the origin of Al-depleted komatiites: Melting experiments of hydrous pyroxene with REE's at high pressure. *Earth and Planetary Science Letters*, 177, 81–87.
- Kato, T., Irifune, T., and Ringwood, A.E. (1987) Majorite partition behavior and petrogenesis of the Earth's upper mantle. *Geophysical Research Letters*, 14,

- 123–145.
- Kilinc, A., Carmichael, I.S.E., Rivers, M.L., and Sack, R.O. (1983) The ferric-ferrous ratio of natural silicate liquids equilibrated in air. *Contributions to Mineralogy and Petrology*, 83, 136–140.
- Meagher, E.P. (1982) Silicate Garnets. In P.H. Ribbe, Eds., *Orthosilicates*, p. 25–66. Reviews in Mineralogy, Mineralogical Society of America, Chantilly, Virginia.
- Nicholls, I.A. and Harris, K.L. (1980) Experimental rare earth element partition coefficients for garnet, clinopyroxene and amphibole coexisting with andesitic and basaltic liquids. *Geochimica et Cosmochimica Acta*, 44, 287–308.
- Ohtani, E., Kawabe, I., Moriyama, J., and Nagata, Y. (1989) Partitioning of elements between majorite garnet and melt and implications for petrogenesis of komatiite. *Contributions to Mineralogy and Petrology*, 103, 263–269.
- Onuma, N., Higuchi, H., Wakita, H., and Nagasawa, H. (1968) Trace element partitioning between two pyroxenes and the host lava. *Earth and Planetary Science Letters*, 5, 47–51.
- Pearce, N.J.G., Perkins, W.T., Westgate, J.A., Gorton, M.P., Jackson, S.E., Neal, C.R., and Chenerly, S.P. (1997) A compilation of new and published major and trace element data for NIST SRM 610 and NIST SRM 612 glass reference materials. *Geostandards Newsletter*, 21, 115–144.
- Pertermann, M., Hirschmann, M.M., Hametner, K., Gunther, D., and Schmidt, M.W. (2004) Experimental determination of trace element partitioning between garnet and silica-rich liquid during anhydrous partial melting of eclogite. *Geochemistry, Geophysics, Geosystems*, 5, Q05A01, DOI: 10.1029/2003GC000638.
- Salter, V.J.M. and Longhi, J. (1999) Trace element partitioning during the initial stages of melting beneath mid-ocean ridges. *Earth and Planetary Science Letters*, 166, 15–30.
- Salter, V.J.M., Longhi, J.E., and Bizimis, M. (2002) Near mantle solidus trace element partitioning at pressures up to 3.4 GPa. *Geochemistry, Geophysics, Geosystems*, 3, 1038, DOI: 10.1029/2001GC000148.
- Shannon, R.D. (1976) Revised effective ionic radii and systematic studies of interatomic distances in halides and chalcogenides. *Acta Crystallographica*, A32, 751–767.
- van Westrenen, W., Blundy, J.D., and Wood, B.J. (1999) Crystal chemical controls on trace element partitioning between garnet and anhydrous silicate melt. *American Mineralogist*, 84, 838–847.
- van Westrenen, W., Blundy, J.D., and Wood, B.J. (2000) Effect of Fe²⁺ on garnet-melt trace element partitioning: Experiments in FCMS and quantification of crystal-chemical controls in natural systems. *Lithos*, 53, 189–201.
- van Westrenen, W., Blundy, J.D., and Wood, B.J. (2001a) High field strength element/rare earth element fractionation during partial melting in the presence of garnet: Implications for identification of mantle heterogeneities. *Geochemistry, Geophysics, Geosystems*, 2, U33–U51, DOI: 10.1029/2000GC000133.
- van Westrenen, W., Wood, B., and Blundy, J. (2001b) A predictive thermodynamic model of garnet-melt trace element partitioning. *Contributions to Mineralogy and Petrology*, 142, 219–234.
- Walter, M.J., Nakamura, E., Tronnes, R.G., and Frost, D.J. (2004) Experimental constraints on crystallization differentiation in a deep magma ocean. *Geochimica et Cosmochimica Acta*, 68, 4267–4284.
- Wood, B.J. and Blundy, J.D. (2003) Trace element partitioning under crustal and uppermost mantle conditions: The influence of ionic radius, cation charge, pressure, and temperature. In R. Carlson, H.D. Holland, and K.K. Turekian, Eds., *Treatise on Geochemistry*, 2, p. 395–424. Elsevier Pergamon, Amsterdam.
- Woodland, A.B. and Koch, M. (2003) Variation in oxygen fugacity with depth in the upper mantle beneath the Kaapvaal craton, Southern Africa. *Earth and Planetary Science Letters*, 214, 295–310.
- Yurimoto, H. and Ohtani, E. (1992) Element partitioning between majorite and liquid: A secondary ion mass spectrometric study. *Geophysical Research Letters*, 19, 17–20.

MANUSCRIPT RECEIVED SEPTEMBER 21, 2005

MANUSCRIPT ACCEPTED MAY 31, 2006

MANUSCRIPT HANDLED BY THEODORE LABOTKA